Continental J. Applied Sciences
El-Jummah *et al*. (2019) 14 (2): 31 – 49 DOI: 10.5281/zenodo.3370167

Research Article

Numerical Predictions of Impingement Heat Transfer with Obstacles as Turbulators: Conjugate Heat Transfer Computational Fluid Dynamics Procedures

[1]El-Jummah A.M*.,[2]Andrews G.E., and [2]Staggs J.E.J.
[1]Department of Mechanical Engineering, University of Maiduguri, Nigeria
[2]Centre for Integrated Energy Research, University of Leeds, United Kingdom
*Corresponding Author: al-jummah@hotmail.com

Abstract

Impingement heat transfer cooling investigations with obstacles in the gap that are applicable to gas turbine (GT) combustor and turbine blades walls were carried out, using conjugate heat transfer (CHT) and computational fluid dynamics (CFD) codes. The heat transfer enhancing obstacles (or Turbulators) investigated include: rib walls (cross and co-flows), rectangular-fins (cross and co-flows), zigzag (cross-flow), pin-fin(cross-flow) and dimples (direct-flow). All the obstacles were aligned transverse to the direction of the cross-flow on the impingement target surface. The CHT CFD analysis was carried out using ANSYS ICEM and Fluent CFD tools for meshing and numerical calculations, respectively. Only the computational geometries for the rib walls and that for the rectangular-fins were investigated experimentally and were validated elsewhere and the other obstacle geometries were not. But, the methods applied in carrying out the computational works are similar to that investigated experimentally. This work varied the shapes of the obstacles and the results obtained were compared, an indication that the current CHT CFD predictions are possible for future design optimization. A 10 × 10 row of impingement jet holes or air hole density, n of 4306 m^{-2} with ten rows of holes in the cross-flow direction was used for all the obstacles. The impingement hole pitch X to diameter D, X/D and gap Z to diameter, Z/D ratios were also kept constant at 4.66 (15.24/3.27) and 3.06 (10.00/3.27), respectively. The target wall made from Nimonic-75 materials has thickness of 6.35 mm for all geometries; also the obstacles have the same material. The rib and the zig-zag walls are 4.5 mm high and 3.0 mm thick, the pin-fin is cylindrical in shape of 8.6 mm diameter and 8.0 mm high and is the same to that used for the rectangular-fins with 3.0 mm thick, while the depth of the

ISSN: 1597 – 9928. Science and Education Development Inst., Nigeria

dimple obstacle is 4.5 mm with the centre-line diameter of 8.6 mm. The obstacles were equally spaced on the centre-line between each row of impingement jets transverse to the cross-flow. One heat transfer enhancing obstacle was used per impingement jet air hole for the rectangular, circular fins and the dimple, while for the rib wall, is one rib per row of the impingement jet air hole. The CFD calculations were carried out for air coolant mass flux G of 1.08, 1.48 and 1.94 kg/sm^2, which are the high flow rates used for regenerative combustor wall cooling whereby, the outlet air-flow, would pass to a low NO_x combustor flame stabilizer. The pressure loss ΔP and surface average heat transfer coefficient (HTC), h for all the G were predicted, with the rectangular pin in co-flow showing better performance in the results. The comparison showed that for low coolant G, a 10 % increase in the overall surface averaged HTC were predicted for the rectangular fin walls, as compared to the other predicted obstacle geometries and 5 % predicted for the high G. These are the reasons that the predicted thermal gradient for this obstacle indicated lower values, showing adequate cooling.

Keywords: Cooling, code, geometry, transverse, cross-flow, optimization, regenerative.

Received: 15 Nov 2018 Accepted: 02 Jan 2019

Introduction

A major factor in achieving high gas turbine (GT) thermal efficiency is by increasing the exit temperature of the combustion chamber (Figure 1a), which is also the temperature of the gases entering the turbine nozzle guide vanes (Figure 1b). But, this higher turbine entry temperature (TET) that signifies higher GT thermal efficiency is also the most important factor in decreasing the CO_2 emissions that aroused due to natural gas fired industrial gas turbines and in civil aircraft.The maximum operational temperature is limited by two factors: the GT hot components(combustor and turbine blade) materials and cooling of the wall materials (Ito *et al*., 2009 and Schilke, 2004). This work is concerned with the maximization of the GTcomponent:combustor and turbine blade walls cooling using impingement jet heat transfer with an anenhancedtarget wall in the impingement gap. The advantage of maximizing the internal wall cooling is that less film cooling air flow will be required as film cooling air flow deteriorates the thermal efficiency and is due to the compression work of the air, which is not fully recovered in the expansion process.Another effect is that the turbine blade efficiency is deteriorated by the increased aerodynamic losses caused by the presence of the film cooling air.

Impingement air jet cooling is one of the most effective wall cooling technologies (Andrews and Hussain, 1984, Friedman and Mueller, 1951, Kercher andTabakoff, 1970,

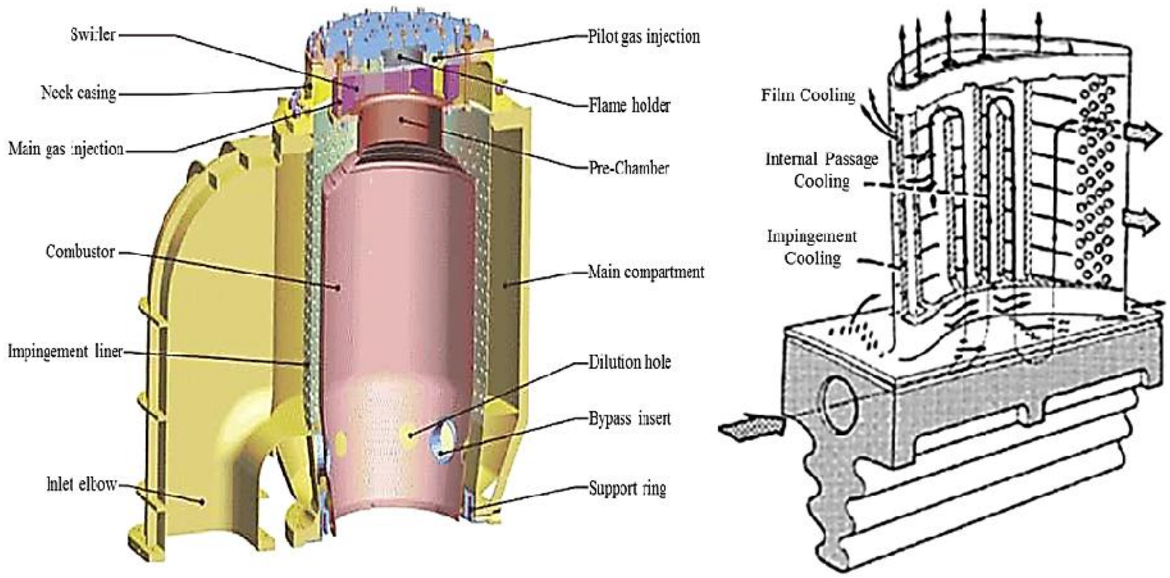

(a) Combustion chamber (Huitenga and Norster, 2014) (b) Turbine blade (Gladden and Simoneau, 1988)

Figure 1: Impingement jet cooling system applied to gas turbine hot wall components

El-jummah *et al*. 2014, Bunker, 2008, Tapinlis*et al*. 2014), it enables the cooling air mass flow to be minimized. For impingement jet cooling without effusion cooling there is a cross-flow in the impingement gap as the air from the first rows of jets flow along the gap to the trailing edge exit and this has been found to reduce the surface heat transfer in the downstream portion of the cooled surface (Andrews and Hussain, 1987). This is a greater problem in wall cooling design for GT combustor walls of Figure 1a, as the distances to be cooled are greater than in the turbine blades of Figure 1b. However, the reasons for this deterioration in heat transfer are not well understood and are often simply ascribed to the deflection of the impingement jet by the cross-flow. This has been predicted by El-Jummah *et al*. (2013, 2013a, b, 2014) using 3D conjugate heat transfer (CHT) computational fluid dynamics (CFD).

CFD investigations of the aerodynamics in the impingement gap show that the effect of cross-flow El-Jummah *et al*. (2013, 2016, 2017, 2018) is more compact and is linked to the movement of impingement jet turbulence. This was shown to cover only the downstream portion of the jet flow and the deflection of the reverse flow jet that reduces the efficient removal of heat from the cooled surface and increases the transfer of heat to the impingement jet surface. The present CHT CFD investigates impingement cooling with obstacles: ribs wall (co- and cross-flows) and rectangular fin (co- and cross-flows), which were investigated experimentally by Andrews *et al*. (2003,

ISSN: 1597 – 9928. Science and Education Development Inst., Nigeria

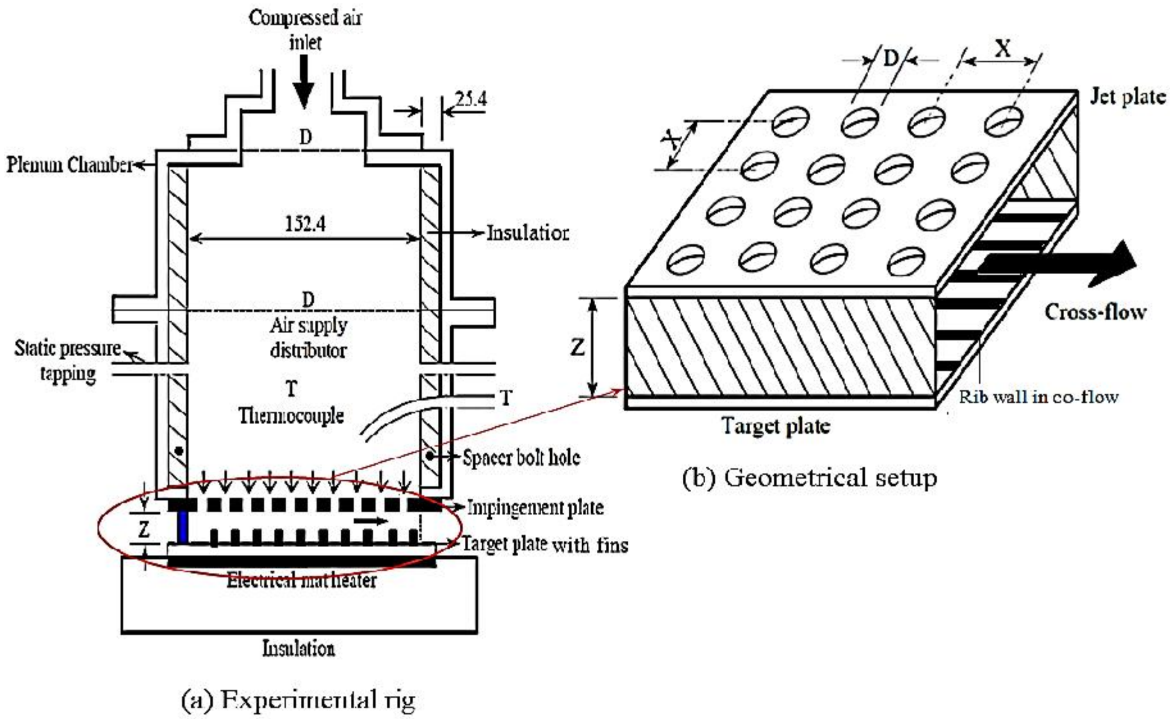

Figure 2: Impingement cooling experimental setup with obstacles on the target surface

2006)and Abdul Hussain and Andrews (1991) using the test rig of Figure2a with the setup shown in 2b. Also investigated and were compared with those shown above,are the previous predictions: pin-fins (cross-flow), zig-zag wall or inclined ribs (cross-flow) and dimple obstacles by El-jummah *et al*. (2019) using the same geometries. The work by El-jummah *et al*. (2017) reviewed different types of obstacles that were either investigated experimentally or numerically, typical of the ones above. This indicates that the use of obstacle to augment GTheat transfer cooling channels is common.The geometries modelled were the same as that used for a smooth target wall El-jummah *et al*. (2013,2014) impingement cooling with a 10 × 10 array of impingement jet holes for a fixed X/D, Z/D, and n of 4.66, 3.06 and 4306 m^{-2}, respectively and are summarized in Table 1. The range of mass flux G that was used for the computation is 1.08 - 1.93 kg/sm^{2}bar as also used by El-jummah *et al*. (2013) for the smooth walls. Each coolant mass flow requires a new computation, but no change in the grid geometry, also new grid geometry is required for each obstacle modelled. The present work on the effect of obstacles in the impingement gap was compared with the predictions for impingement smooth wall cooling, so that the enhancement of heat transfer could be predicted. The

ISSN: 1597 – 9928. Science and Education Development Inst., Nigeria

impingement geometry investigated is typical of low NOx primary zone combustion chamber wall where the impingement efflux is discharged as the main combustion air (Huitenga and Norster, 2014, Reiss *et al*. 2014), as shown in Figure 1a. Impingement jet cooling is also used for cooling combustor transition ducts or for the primary low NOx region only and then the jet air is passed into combustor as film cooling or as part of the dilution air, this method of primary zone cooling is used in several industrial and aero gas turbine engines.

Table 1: Impingement jet cooling geometrical parameters

Variables	Dimensions
D (mm)	3.27
X (mm)	15.24
Z (mm)	10.0
L (mm)	6.35
L/D	1.94
X/D	4.66
Z/D	3.06
X/Z	1.52
N	4306 m^{-2}
Array	10 × 10

Table 2: Obstacle walls parameters

Types	W or D_o mm	H or δ mm	t mm	H/W δ/D_o
Rectangular fin: cross-flow	Continuous	4.50	3.0	
Rectangular fin : co-flow	Continuous	4.50	3.0	
Rib wall: cross-flow	8.59	8.00	3.0	0.93
Rib wall: co-flow	8.59	8.00	3.0	0.93
Zigzag (or inclined) wall: cross-flow	Continuous	4.50	3.0	
Pin-fin: cross-flow	8.59	8.00	-	0.93
Dimple: direct-flow	8.59	2.58	-	0.30

ISSN: 1597 – 9928. Science and Education Development Inst., Nigeria

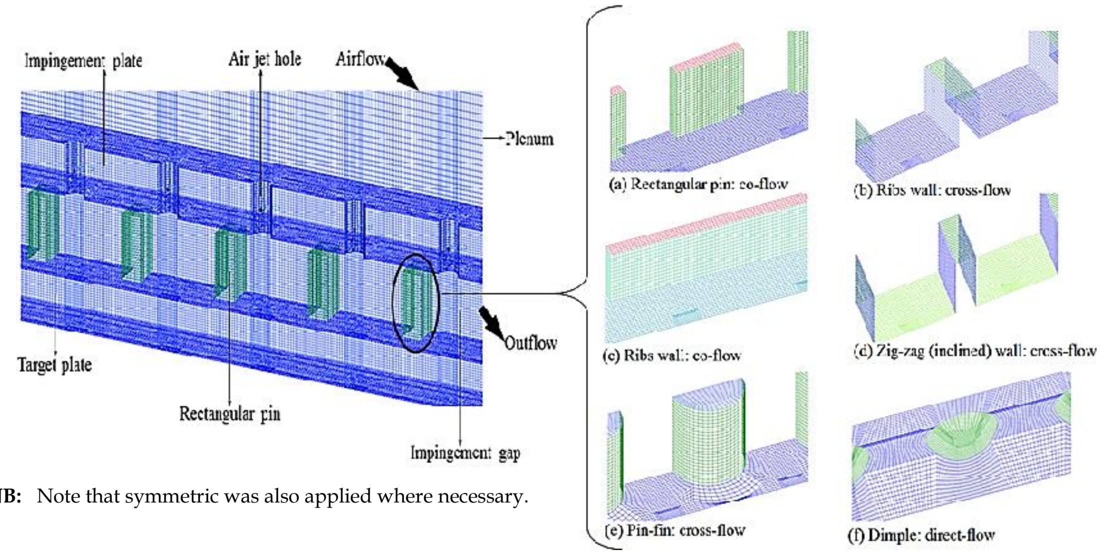

NB: Note that symmetric was also applied where necessary.

Figure 3: The impingement jet grid geometry with obstacles on the target surface

CFD Methodology

Model Grid Geometry

Table 1shows the geometrical parameters that were used in modeling the impingement cooling geometry of Figure 3 (left) and was the same method as that modelled by the work of El-jummah *et al*. (2013) for smooth target walls. This work investigates the potential improvement in the heat transfer using obstacles in the impingement gap, as summarized in Figure 3 left with the dimensions shown in Table 2. The rectangular fin (Figure 3a) was H of 80% Z with equal fin width W and pin gap, the rib wall (Figure 3b and c) thickness t, is 3mm and it consists of a continuous wall of height H that was 45% Z: both were previously investigated experimentally. In addition, three alternative heat transfer enhancements were also modeled with the same impingement configuration of Table 1 and Figure 3 (right) shown. These include cylindrical pin-fin in cross-flow of the same properties with the rectangular pin, zig-zagor inclined wall in cross-flow with properties of rib wall and dimples of depth δ of 2.58 mm (Xie *et al*., 2013) and diameter d_o that is the same to the pin-fin, with the gap fixed at 100 % of Z. The approach that was used to model the zig-zig obstacle of Figure 3d is similar to that used experimentally for inclined ribs by Wang *et al*. (1998). The fin was essentially a modification of the straight ribs (Andrews *et al*., 2006) but was only used with cross-flow. The half circular pin-fin obstacle of Figure 3e has all its variables the same as the rectangular pin: cross-flow obstacle of Andrews *et al*. (2006), whereby the width is the pin-fin diameter D_o and fixed at the same height H.

ISSN: 1597 – 9928. Science and Education Development Inst., Nigeria

Table 3: Percentage of grid cells in the modelled geometry for $y^+ \sim 35$

Types	Parts (%)				
	Test walls	**Obstacles**	**Gap**	**Holes**	**Plenum**
Rectangular fin: cross-flow	28.5	7.2	20.6	8.4	35.3
Rectangular fin : co-flow	28.5	7.2	20.6	8.4	35.3
Rib wall: cross-flow	28.5	8.1	19.7	8.4	35.3
Rib wall: co-flow	28.5	8.1	19.7	8.4	35.3
Zigzag (or inclined) wall: cross-flow	28.5	8.3	19.5	8.4	35.3
Pin-fin: cross-flow	26.5	6.7	23.4	8.1	35.3
Dimple: direct-flow	22.8	5.7	27.4	8.8	35.3

The computational grids geometries (Figure 3) were modelled using ANSYS ICEM version 13. The number of gridcells in the plenum for all the obstacles geometries modeled were fixed at 35.3 % of the total, as Table 3 show, implying that 64.7 % of the grid cells are in the test and obstacle walls, gap and holes.Apart from the dimple obstacles, every other obstacle grids are in the region of the impingement gap, hence the obstacle solid walls formed part of the impingement gap fluid region, as in Table 3and so fluid grids are now solid one. The dimple obstacle of Figure 3c formed part of the depth of target solid wall, which resulted in the impingement gap fluid grids replacing the region of the solid grids. This increases the impingement gap cell size and reduced the target wall cells as a proportion of the total computational cells, as shown in Table 3. The dimple target surface was modelled with the dimples in-line with the air jets, while the other obstacles were placed between rows of jetholes.

Computational Procedures

The present CHT CFD numerical investigations for the type of obstacles modelled were computed for varied G of 1.08, 1.48 and 1.98 kg /sm^{2}bar, which imply that for each obstacle, three computations were carried out and were based on the grids modelled geometries. The standard k - ε turbulence model in ANSYS Fluent was used with a wall function y^+ value ~35, as shown in Table 3. This y^+ value was in the range of the near wall, law of the wall of $30 < y^+ < 300$ with the computational procedure the same as that previously validated. This was because the flow aerodynamics in the impingement gap are major aspects of the flow that are characterized with strong flow recirculation for which the k-ε model has good prediction capabilities. Table 4 below shows the computational flow boundary conditions that were applied in the numerical calculations and are the same flow conditions used by El-jummah *et al.*(2013). The

ISSN: 1597 – 9928. Science and Education Development Inst., Nigeria

Table 4: Computational flow parameters and the boundary conditions

G (kg/sm²bar)	**1.93**	**1.48**	**1.08**
V_j(m/s)	43.41	33.5	24.3
U_c(m/s)	24.0	18.4	13.4
V_j/U_c	1.8	1.8	1.8
Re_h(= °$V_j D$/«)	9680	7440	5400
T_∞(K)	288	288	288
T_w(K)	353	353	353
ρ (kg/m³)	1.225	1.225	1.225

convergence criteria were set at 10^{-5} for continuity, 10^{-11} for energy and 10^{-6} for k, ε and momentum (x, y and z velocities), respectively.

Results and Discussion

Predictions of the Axial Pressure Loss Profiles

The aerodynamics in the impingement gap is complex,as was previously predicted by the work of El-jummah *et al.* (2013a) using CHT/CFD modelling. The additions of obstacles to the target wall were aimed at increasing the heat transfer by inserting obstacles (or turbulators) at the location of the reverse flow between each impingement jet flow. This increases the complexities of the aerodynamics as the cross-flow in the gap builds up with succesive rows of impingement jets.The cross-flow obstacles create a blockage to the impingement gap cross-flow, which increases the pressure loss ΔP due to the increased cross-flow at upstream exit jet holes along the gap, as shown in Figure4a.Therefore, this leads to the increased flow mal-distribution (or normalized velocity) between the impingement holes for all the obstacle cross-flow configurations, as in Figure 4b and this is the basis of the blockage in gap cross-flow. Figure 4a and b also shows that the co-flow obstacles and the dimplein direct flow have a flow mal-distribution and ΔP similar to the smooth wall predicted by El-jummah *et al.* (2014), which should be based on the minimum blockage of the impingement gap cross-flow. However, the reduced pressure loss and flow mal-distribution for co-flow with ribs and rectangular fin were unexpected. It appears that as the rib prevents the flow of adjacent air jets in the transverse direction, it also changes the reverse flow jet in a way that reduces its impact on the upstream hole scross-flow pressure loss.

ISSN: 1597 – 9928. Science and Education Development Inst., Nigeria

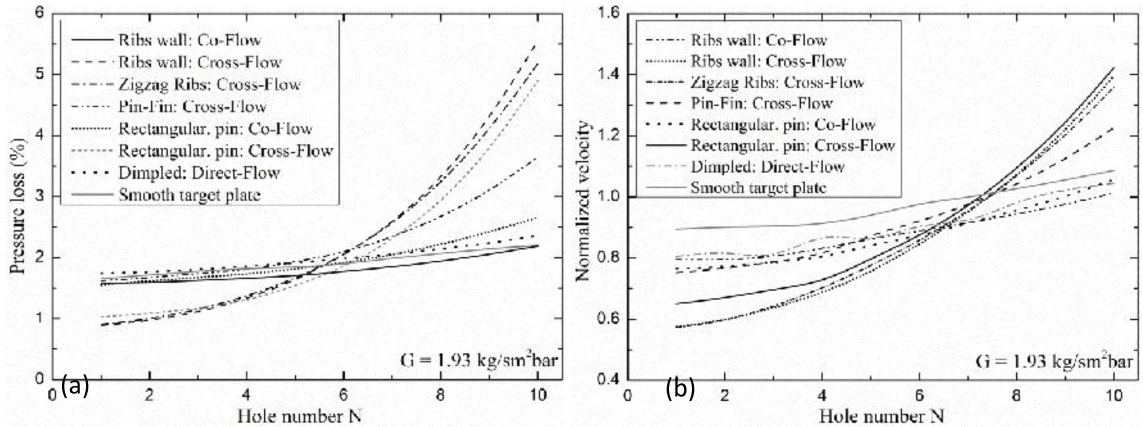

Figure4: Comparison of predicted jet holes aerodynamics along the impingement gap

$$h = \frac{q''}{(T_s - T_\infty)} \quad (1)$$

Predictions of the Surface and Locally X² Average Heat Transfer Coefficient

Equation 1 is used in predicting the surface and X^2average HTC on the target wall, whereby the whole target surface and the area (or X^2) region of the jet flow on the target wall, respectively were captured. The complex interactions of the jets along the impingement gap cross-flow with the addition of the obstacle walls, is expected to exhibit similar trend to the impingement heat transfer situations. This was reported by El-jummah *et al*. (2017, 2018), which this work also follows the same techniques in capturing the data. Figure 5a compares the predicted target surface average HTC for all the obstacles investigated and compares them with the smooth wall HTC predictions, also shown is Figure 5b, which is the impingement jet surface average HTC.

Figure 5a shows that the rectangular fin in co-flow had the greatest improvement on the smooth wall surface average HTC. However, this improvement was only 20% at low G and 5% at high G and could be based on the fact that the disruption of this obstacle along the gap is where the gap cross-flow significantly reduces the heat transfer; hence the HTC increased was seen there. Two of the obstacle surfaces were predicted to have lower surface average HTC than the smooth target surface and these were the rectangular fin in co-flow and the dimple in direct flow. The rectangular fin results are unexpected, as is the obstacle that creates the greatest turbulence (El-jummah *et al*., 2018) with increased pressure loss. For the dimple surface, the action created a stronger recirculation flow in the gap and had also remove the wall airjet

ISSN: 1597 – 9928. Science and Education Development Inst., Nigeria

interaction on the target surface, thereby generating less turbulence on the surface with lesser heat transfer. However, other investigators have shown a benefit of dimple surfaces experimentally (Xie*et al*., 2014), but this is not predicted for the X/D = 4.66 and 10mm impingement gap that was modelled in the present work.The comparison of the predicted surface average HTC on the impingement jet wall,as shown in Figure 5bfor all the obstacles modelled, shows the indication that the reversed jets heats up the impingement jets wall.Figure 5b clearly signifies that any of the obstacles predicted surface average HTC that is lower in Figure 5a,was the impact ofthe extracted heat by the jets wall.

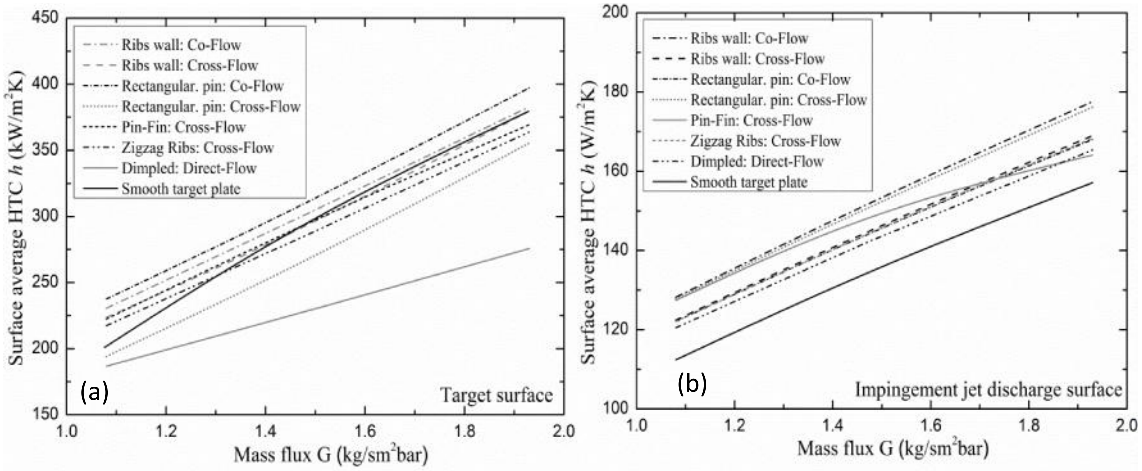

Figure 5: Comparison of predicted target and impingement surface HTC for varied G

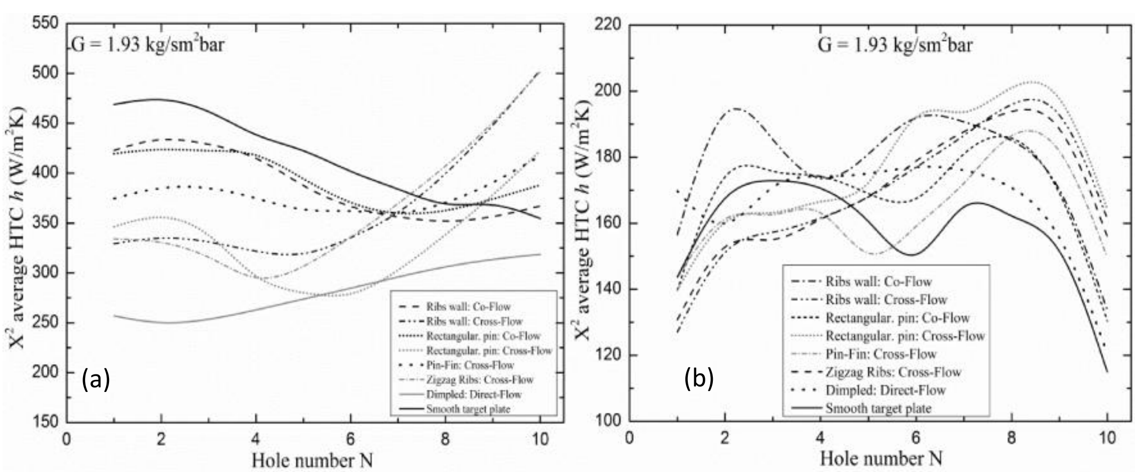

Figure 6: Comparison of predicted target and impingement jet locally X^2 average HTC, *h*

ISSN: 1597 – 9928. Science and Education Development Inst., Nigeria

Figure 6a shows the predicted X^2 average HTC as a function of distance (or hole) along the target wall for all the obstacles modelled, their effects were also compared with the trend for the smooth wall. Also shown in Figure 6is the predicted influence of obstacles in the gap that is predominantly on the axial variation of the locally X^2surface average HTC, which resulted in heating up the impingement jet walls (see 6b), as also shown and described in Figure 5b. Note that the data shown in Figures5a and 6a do not include the obstacle HTC, as were predicted in Figure 7 and 8using Equations 2 and 3, respectively to have most of the heat. Therefore, only the region of the target wall as conducted experimentally by Andrews *et al*. (1988) that the data was extracted from the CFD predictions. The increased flow in the downstream jets is part of the reason why the ribs with cross-flow geometries, as Figure 6a shows have the highest HTC in the downstream part of the target wall, compared with the opposite trend for the smooth wall. All the co-flow geometries showed a similar trend to that of the smooth wall with a decreased HTC along the distance and the highest HTC at the leading section of the target wall.

A feature of the experimental results that was reproduced in the predictions is that for the co-flow results with the gap cross-flow having a clear channel flow between the obstacles, the trend of the local average results is for the HTC to decline with distance, as seen for the smooth wall. However, with the cross-flow obstacle configuration there is no clear passage for the gap cross-flow and this changes the axial variation of locally X^2 surface average HTC with distance. Now the HTC increases in the trailing edge region instead of decreasing. This effect is shown in Figure 7 to be greatest for the continuous rib (plus the inclined) in cross-flow. Thus the main effect of the obstacles is to remove the feature of the smooth wall geometry that led to the local surface average HTC deteriorating with distance along the impingement target surface. This must be the reason why in Figure 6b, the region of the upstream last holes had the lowest HTC, which indicates heating there is low as it has been mostly extracted out by the obstacles.

$$Nu = \frac{hD}{k_f} \quad (2)$$

$$T^* = \frac{(T - T_\infty)}{(T_w - T_\infty)} \quad (3)$$

ISSN: 1597 – 9928. Science and Education Development Inst., Nigeria

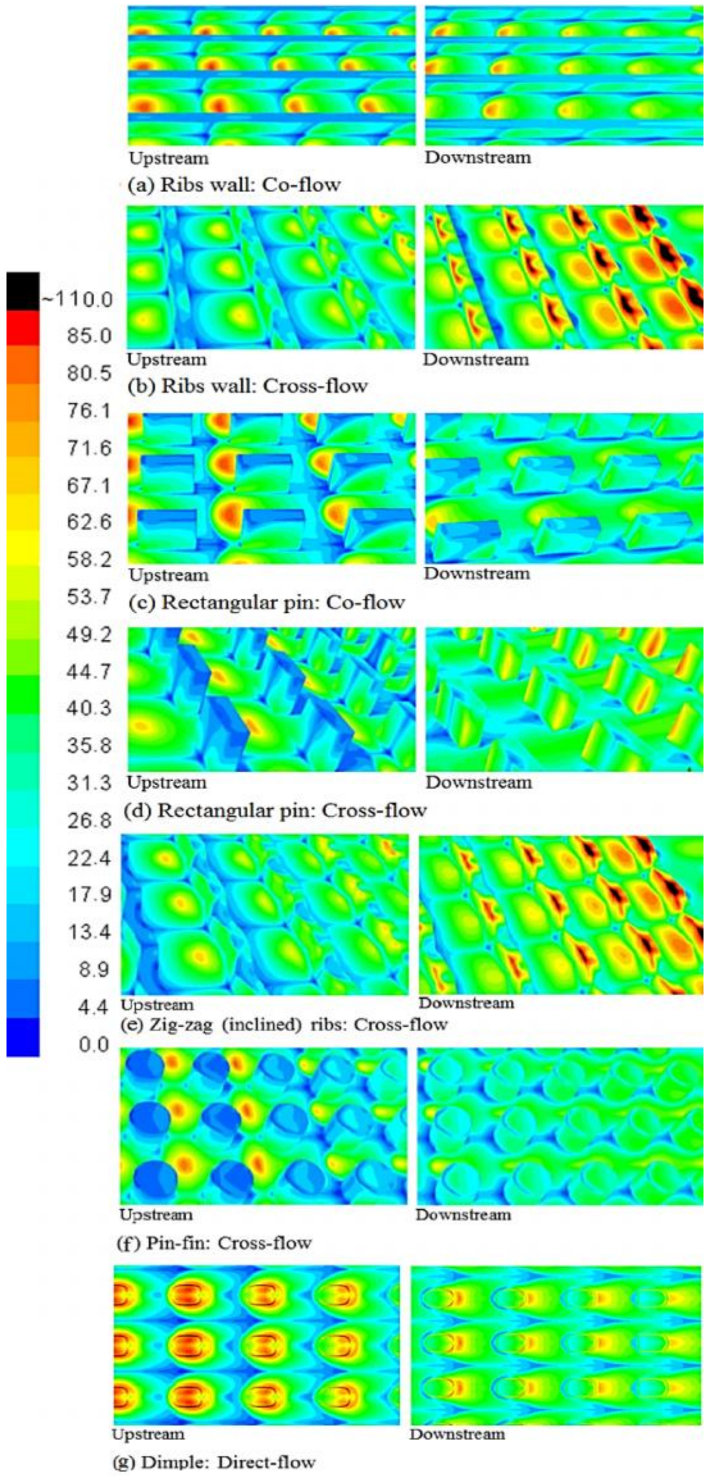

Figure 7: Contours of Nusselt number on the target surface for G of 1.93 kg/sm^{2}bar.

ISSN: 1597 – 9928. Science and Education Development Inst., Nigeria

Distribution of Target Surface Nusselt Number

Figure 7 (a - g) shows the CHT CFD predicted target surface distribution of Nusselt number, Nu and was predicted using Equation 2, for all the obstacles modelled. Figure7 shows that the smooth wall results are difficult to improve on and all the obstacle surface distributions Nu show lower values in the region of only the target surface (excluding the obstacles) than were expected. Any enhancement of heat transfer has to come from the heat transfer to the rib or fin or dimple surfaces, which is clearly shown by the obstacles in Figure 7. The quite poor Nu distribution for the fins in cross-flow and dimple in direct flow on the target surface are partially compensated for by the heat transfer on the fin surface, which extract heat from the target surface by conduction. For the co-flow fins, the HTC behavior on the target surface seems quite similar to the smooth target predicted by El-jummah *et al*. (2014) and its impact on the fins was therefore reduced.For the dimple obstacle, the movement of the jets around the vicinity of the dimple and on the target surface along the downstream leads to deterioration in heat transfer and it also creates horseshoe vortices that are seen in Figure 7g.

Heating of the Impingement Target Wall

The effects of reverse flow by impingement air jet on the jetsplate, which also causes heating of the plate has previously been reported (El-jummah *et al*., 2013, 2014) and has been shown to influence the cooling of the target walls. The dimensionless temperatures $T^*$of Equation 3 was used to predict the target wall and the coolant air temperatures through the impingement gap. Figure 8 (a - g) is the coolant air T^* for all the obstacle geometries modelled and are flow in the symmetry planes between row of impingement holes for G = 1.93 kg/sm^{2}bar. These clearly show the image of the reverse flow heated jets and the cooled zones of the obstacle walls: region where the severity that affects the adequate and uniform cooling of the target wall is seen (Figure 8). The presence of the obstacles influences more the deflection of there verse flow jets by the gap cross-flow, which does not, impinges on the target surface but on the fins. Also the heated reverse flow jets that were from the impingement jet wall impinges back to the jets air and to the target surface, hence causing heating effects on them. This could be the reason why the thermal gradient of Figure 9a has little effects to target walls, which also shows the influence of the high jet flow interactions between the jet plates and the obstacle walls.

ISSN: 1597 – 9928. Science and Education Development Inst., Nigeria

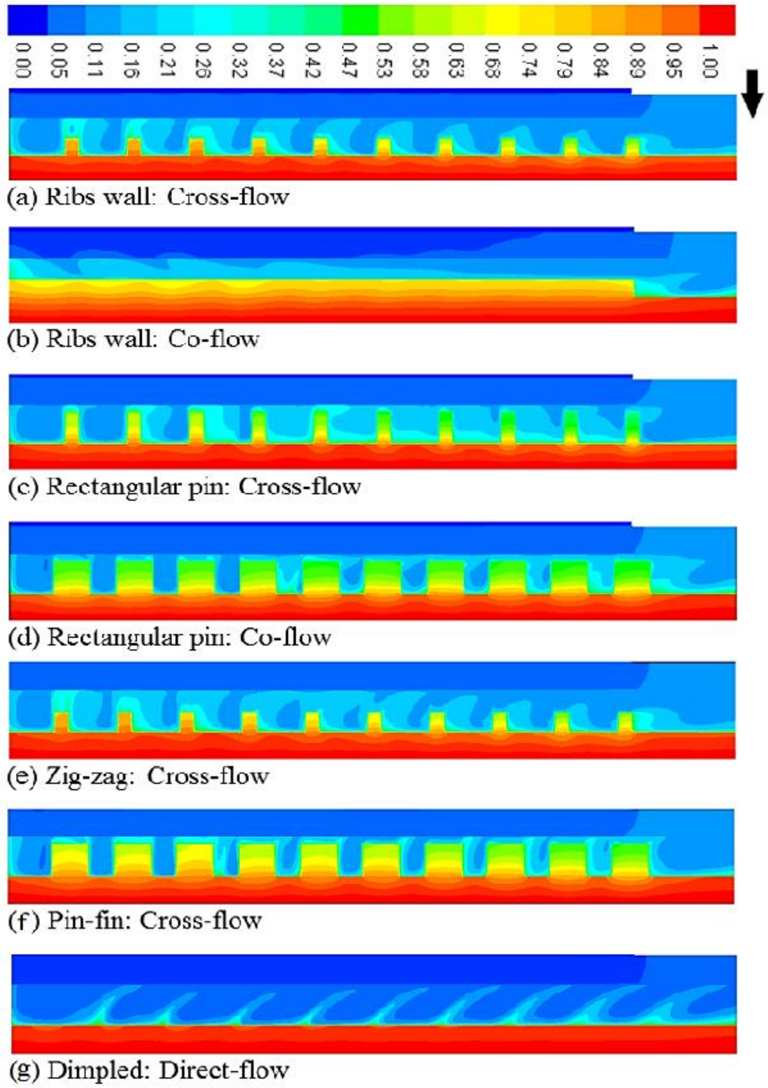

Figure 8: Contours of normalized T^*in the impingement gap for G of 1.93 kg/sm²bar

Prediction of the Thermal Gradients in the Target and Fin Walls

Figure 9a shows the thermal gradients through the combined target and obstacle walls for the obstacles at hole 9 position, the smooth wall predictions are shown for comparison and were predicted using Equation 3. This is the location where the exit impingement gap pressure loss shown in Figure 9b controls the gap cross-flow that was largely agreed to influence the deterioration of heat transfer.The lowest thermal gradients T^* for all the obstacles modelled were predicted to be in the region close to the jet plates. The obstacles in the cross-flow configuration gave lower thermal

ISSN: 1597 – 9928. Science and Education Development Inst., Nigeria

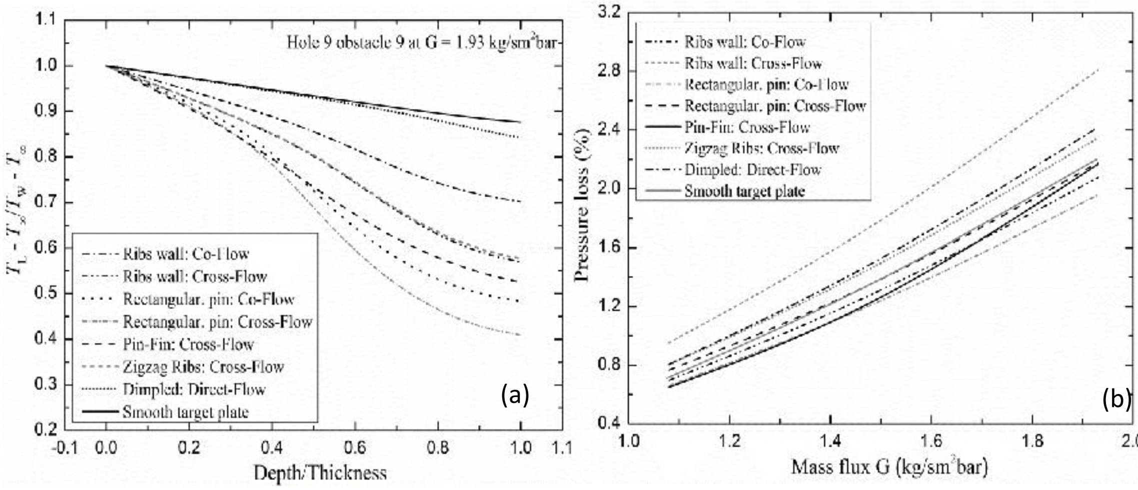

Figure 9: The predicted effects of air jet flow complexities along impingement gap

gradients followed by the co-flow ones. The dimple in direct flow gave the worse thermal gradient and is shown to be in the same trend and date with the smooth target wall. The thermal gradients result indicates that the higher the HTC and turbulence, the lower will be the wall thermal gradient and the better is the surface cooling. Therefore, any decrease in surface or locally X^2 average HTC with obstacles, results in an increase in the thermal gradient across the wall thickness.

Conclusions

The predictions showed that it was difficult to enhance the smooth wall impingement heat transfer and that obstacles could also deteriorate heat transfer, as does the gap flow cross-flow.

The main effect of the obstacles was to enhance the heat transfer to the impingement jet wall and decrease it to the target wall. A small increase in the overall surface average heat transfer was predicted for the co-flow configuration with fins.

TheCFD techniques applied in the present work show that gas turbine cooling system can be optimized using CHT CFD design codes.

ISSN: 1597 – 9928. Science and Education Development Inst., Nigeria

Nomenclature

A	Impingement hole porosity $((\pi/4)\ D^2)/X^2$	T_∞	Coolant temperature, 288K
D	Impingement air hole diameter, m	T^*	Normalized mean temperature
D_o	Obstacle diameter, m	T_S	Target surface metal wall temp., K
G	Coolant Mass flux, kg/sm²bar	T_w	Target wall imposed temp. (360K)
h	Heat transfer coefficient (HTC), W/m²K	V_j	Impingement jet mean velocity, m/s
H	Obstacle height, m	v	Kinematic viscosity, m²/s
k_f	Thermal conductivity of fluid, W/mK	W	Obstacle width, m
L	Test wall metal thickness, m	X	Hole to hole pitch, m
N	Number of jet/unit surface area, m^{-2}	Z	Plate to plate gap, m
N	Number of upstream rows of imp.holes	ξ	Grid cell size, m
Nu	Nusselt Number	δ	Obstacle depth, m
ρ	Density of air, kg/m³		
ΔP	Impingement wall pressure loss, Pa		
P	Coolant supply static press. (app. 1bar)		
Pr	Prandtl number		
Re	Reynolds number		
t	Obstacle thickness, m		

Subscripts

avg	average	*f*	fluid
L	Local	∞	Coolant
C	cross-flow	o	Obstacle
j	Jet	W	Wall
s	Surface		

References

Abdul Husain R. A. A. and Andrews G. E. (1991). Enhanced Full Coverage Impingement Heat Transfer With Obstacle in the Gap. *Proc. ASME Int. Gas Turbine & Aeroengine Congress & Eposition,* 91-GT-346**,** 1 - 12.

Andrews G. E. and Hussain C. I. (1984). Impingement Cooling of Gas Turbine Components. *High Temperature Technology,* 2 (2)**,** 99 - 106.

Andrews G. E. and Hussain C. I. (1987). Full Coverage Impingement Heat Transfer: The Influence of Cross-Flow. *AIAA/SAE/ASME/ASEE 23rd Joint Propulsion Conference,* AIAA-87-2010**,** 1 - 9.

Andrews G. E., Abdul Husain R. A. A. and Mkpadi M. C. (2003). Enhanced Impingement Heat Transfer: Comparison of Co-Flow and Cross-flow with Rib Turbulators. *Proc. GTSJ Int. Gas Turbine Congress,* IGTC TS-075 1 - 8.

Andrews G. E., Abdul Husain R. A. A. and Mkpadi M. C. (2006). Enhanced Impingement Heat Transfer: The Influence of Impingement X/D for Interrupted Rib Obstacles (Rectangular Pin Fins). *Trans. ASME J. Turbomachinery,* 128**,** 321 - 331.

ISSN: 1597 – 9928. Science and Education Development Inst., Nigeria

Bunker R. S. (2008). The Effects of Manufacturing Tolerances on Gas Turbine Cooling. *Proc ASME Turbo Expo,* GT-50124**,** 1 - 16.

El-jummah, A. M., Abdul Hussain R. A. A., Andrews G. E. and Staggs J. E. J. (2013). Conjugate Heat Transfer CFD Predictions of the Surface Averaged Impingement Heat Transfer Coefficients for Impingement Cooling with Backside Cross-flow. *Proc. ASME IMECE Conference,* IMECE-63580**,** 1 - 14.

El-jummah, A. M., Andrews, G. E. and Staggs, J. E. J. (2013a). Conjugate Heat Transfer CFD Predictions of Impingement Jet Array Flat Wall Cooling Aerodynamics with Single Sided Flow Exit. *Proc. ASME Turbo Expo Conference,* GT-95343**,** 1 - 12.

El-jummah, A. M., Andrews, G. E. and Staggs, J. E. J. (2013b). Conjugate Heat Transfer CFD Predictions of the Influence of the Impingement Gap on the Effect of Cross-Flow. *Proc. ASME Heat Transfer Conference,* HT-17180**,** 1 - 12.

El-jummah A. M., Abdul Hussain R. A. A., Andrews G. E. and Staggs J. E. J. (2014). Conjugate Heat Transfer Computational Fluid Dynamic Predictions of Impingement

Heat Transfer: The Influence of Hole Pitch to Diameter Ratio X/D at Constant Impingement Gap Z. *Trans. ASME J. Turbomachinery,* 136 (12)**,** 1 - 16.

El-jummah A. M., Andrews G. E. and Staggs J. E. J. (2016). Impingement Jet Cooling with Ribs and Pin Fin Obstacles in Co-flow Configurations: Conjugate Heat Transfer Computational Fluid Dynamic Predictions. *Proc. ASME Turbo Expo: Turbomachinery Technical Conference & Exposition,* GT- 57021**,** 1 - 15.

El-jummah A. M., Oluwole F. A., Andrews G. E. and Staggs J. E. J. (2017). Numerical Predictions of Enhanced Impingement Jet Cooling with Ribs and Pin Fin in Co-flow and Cross-flow Configurations. *Arid Zone Journal of Engineering, Technology and Environment (AZOJETE),* Vol. 13 (1)**,** 149 - 162.

El-jummah A. M., Andrews G. E. and Staggs J. E. J. (2018). Enhancement of Impingement Heat Transfer with the Cross-flow Normal to Ribs and Pins between each Row of Holes. *Proc. ASME Turbo Expo: Turbomachinery Technical Conference and Exposition,* GT - 76969**,** 1 -12.

ISSN: 1597 – 9928. Science and Education Development Inst., Nigeria

El-jummah A. M., Andrews G. E. and Staggs J. E. J. (2019). Predictions of Impingement Heat Transfer with Dimples, Pin-fins and zig-zag rib Obstacles: Conjugate Heat Transfer Computational Fluid Dynamics Predictions. *Proc. ASME Turbo Expo: Turbomachinery Technical Conference and Exposition,* GT-90730**,** 1 -12.

Friedman S.J. and Mueller A.C. (1951). Heat Transfer to flat surfaces *Proc. IMechE: General Discussions on Heat Transfer***,** 138 - 142.

Gladden H. J. and Simoneau R. J. (1988). Review and Assessment of the Database and Numerical Modelling for Turbine Heat Transfer. *Proc. ASME Turbo Expo,* 2.

Huitenga H. and Norster E. R. (2014). Development Approach to the Dry Low Emission Combustion System of MAN Diesel & Turbo Gas Turbines. *Proc. ASME Turbo Expo,* GT-25164**,** 1 - 10.

Ito E., Okada I., Tsukagoshi K., Muyama A. and Masada J. (2009). Development of Key Technologies for the Next Generation 1700 C-Class Gas Turbine. *Proc. ASME Turbo Expo,* GT-59783**,** 1 - 11.

Kercher D. M. and Tabakoff W. (1970). Heat Transfer by a Square Array of Round Air Jets Impinging Perpendicular to a Flat Surface Including Effect of Spent Air. *Trans. ASME J. Eng. Power***,** 73 - 82.

Reiss F., Wiers S-H., Orth U., Aschenbruck E., Lauer M. and El Masalme J. (2014). Combustion System Development and Testing for MAN's New Industrial Gas Turbines MGT 6100 and MGT 6200. *Proc. ASME Turbo Expo,* GT-25907**,** 1 - 9.

Schilke P. W. (2004). Advanced Gas Turbine Materials and Coatings. *General Electric Company GE Energy,* GER-3569G [08/04]**,** 1 - 25.

Tapinlis O., Choi M., Gillespie D. R. H., Lewis L. V. and Ciccomascolo C. (2014). The Effect of Impingement Jet Heat Transfer on Casing Contraction in a Turbine Case Cooling System. *Proc. ASME Turbo Expo,* GT-26749**,** 1 - 11.

Wang Z., Ireland P. T., Kohler S. T. and Chew J. W. (1998). Heat Transfer Measurements to a Gas Turbine Cooling Passage With Inclined Ribs. *Trans. ASME J. Turbomachinery,* 120**,** 63 - 69.

Xie Y., Li P., Lan J. and Zhang D. (2013). Flow and Heat Transfer Characteristics of Single Jet Impinging on Dimpled Surface *Trans. ASME J. Heat Transfer,* 135**,** 1 - 15.